

# Overcoming the fundamental limit of quantum transduction via intraband entanglement

Haowei Shi<sup>1,\*</sup> and Quntao Zhuang<sup>1,2,†</sup>

<sup>1</sup>*Ming Hsieh Department of Electrical and Computer Engineering,  
University of Southern California, Los Angeles, California 90089, USA*

<sup>2</sup>*Department of Physics and Astronomy, University of Southern California, Los Angeles, California 90089, USA*

A quantum transducer converts an input signal to an output probe at a distant frequency band while maintaining the quantum information with high fidelity, which is crucial for quantum networking and distributed quantum sensing and computing. In terms of microwave-optical quantum transduction, the state-of-the-art quantum transducers suffer low transduction efficiency from weak nonlinear coupling, wherein increasing pump power to enhance efficiency inevitably leads to thermal noise from heating. Moreover, we reveal that the efficiency-bandwidth product of a cavity electro-optical or electro-optomechanical transducer is fundamentally limited by pump power and nonlinear coupling coefficient, irrespective of cavity engineering efforts. To overcome this fundamental limit, we propose to noiselessly boost the transduction efficiency by consuming intraband entanglement (e.g., microwave-microwave or optical-optical entanglement in the case of microwave-optical transduction). Via a squeezer-coupler-antisqueezer sandwich structure, the protocol enhances the transduction efficiency to unity in the ideal lossless case, given an arbitrarily weak pump and nonlinear coupling. In practical cavity systems, our entanglement-assisted protocol surpasses the non-assisted fundamental limit of the efficiency-bandwidth product and reduces the threshold cooperativity for positive quantum capacity by a factor proportional to two-mode squeezing gain. Given a fixed cooperativity, our approach increases the broadband quantum capacity by orders of magnitude.

## I. INTRODUCTION

Quantum transduction aims to interconnect quantum computers and processors via converting quantum states between different frequencies [1–3]. It serves as the hinge between the microwave superconducting qubits and the optical telecommunication photons, enabling robust quantum networking [4–7], and ultimately distributed quantum sensing [8] and distributed quantum computing [9, 10]. Despite the proposals based on various physical platforms [11–27], current quantum transduction systems are still far from satisfying, hindered by a conundrum to balance transduction efficiency, pump-induced heating, and bandwidth [26, 28–32].

An ideal transducer has unity transduction efficiency, zero added noise, and large bandwidth. As one-way quantum communication is forbidden for efficiency below 50% [33], remarkable efforts have been made to improve the on-resonance transduction efficiency to  $> 50\%$ . For example, the recent progress in electro-optomechanical transducers [11, 34] adopts extremely high-Q mechanical resonators as a mediating mode to connect the microwave mode and the optical mode, which achieves the highest transduction efficiency up to 47% so far with 3.2 noise photons [30]. However, such mediation boosts the on-resonance efficiency at the cost of bandwidth, e.g. the bandwidth is limited to 2 kHz in Ref. [30], c.f. typical bandwidth  $\sim 10$  MHz of direct conversion [29, 35]. In fact, the bandwidth of an electro-optomechanical trans-

ducer is limited below the mechanical resonance frequency  $\sim$  MHz, which must operate at the resolved sideband limit to suppress the undesired blue sideband two-mode squeezing noise [30, 36]. GHz piezo-optomechanical transducers [19, 26] offer room-temperature broadband transduction, but the transduction efficiency is limited, e.g.  $\sim 10^{-5}$  in Refs. [19, 26], due to the optical absorption heating of mechanical resonators [37]. The direct electro-optical conversion [15, 16] is free from the complications due to the mechanical mode, whereas its transduction efficiency is still limited [17, 28]. Pulsed pumping has been demonstrated to mitigate the heating and further boost the instantaneous nonlinear coupling for piezo-optomechanical transduction [26] and direct electro-optical transduction [29, 35], however its low duty cycle drastically reduces the transduction rate and it is incompatible with continuous-wave signals.

Such a tradeoff between the transduction efficiency and bandwidth is inevitable. In this paper, we reveal that the efficiency-bandwidth product [38] (EBP) of cavity electro-optical or electro-optomechanical transduction, and any transduction with similar Hamiltonian, is fundamentally limited by the nonlinear coupling coefficient and pump amplitude, regardless of the linewidths of cavities. Unfortunately, the nonlinear coupling between photons is intrinsically weak, and a stronger pump inevitably induces more thermal noises. Therefore, besides the endeavor in materials science and nanofabrication, paradigm shifts are needed to boost quantum transduction and overcome the limit.

Recently, there have been theoretical efforts towards this goal. For example, one can utilize the conventionally discarded environment output to correct the transducer imperfection, via adaptive control [39] or Gottesman-

\* hwshi@usc.edu

† qzhuang@usc.edu

Kitaev-Preskill (GKP) encoding [40]. However, the adaptive control protocol relies on ultra-precise broadband homodyne measurement and adaptive displacement in addition to inline squeezing; the state-of-the-art systems for GKP state engineering [41] are far from usable. In addition, the GKP qubit encoding of the input quantum information is not compatible with continuous-variables. Other approaches rely on cross-band microwave-optical entanglement [32, 42] to enable the teleportation-based transduction approach [25, 43]; however, noiseless teleportation requires high fidelity cross-band entanglement and thus extremely high pump power along with the heating issue as challenging as the direct frequency conversion.

In this work, we propose an intraband-entanglement-assisted protocol to achieve a noiseless broadband enhancement in the efficiency of weak signal transduction between arbitrary distant frequencies, therefore overcome the fundamental limitation on EBP. The proposed protocol is inspired by entanglement-assisted sensing [44] and only requires intraband (optical-optical or microwave-microwave) entanglement as shown in Fig. 1(a)(b), distinct from teleportation which requires cross-band entanglement, measurement and conditional operation. In the absence of loss, for an arbitrarily weak nonlinear coupling, the transduction efficiency can always be enhanced up to unity without any added noise. In the next section, we provide an overview of the protocol and its quantum advantage.

## II. OVERVIEW

Entanglement assistance is known as a powerful resource that enhances the precision of weak signal detection beyond the standard quantum limit (SQL) in various scenarios, e.g. nonlinear interferometry [45, 46], quantum illumination radar [47] and dark matter search [44, 48], via combining two-mode squeezing and antisqueezing before and after the sensing process. The quantum advantage has been demonstrated experimentally using photonic ancilla [49, 50] and spin ancilla [51]. In this paper, we exploit entanglement assistance to boost quantum transduction.

The entanglement-assisted protocol is shown in Fig. 1. Our protocol features an ancilla entangled with the output at the same frequency band, e.g. at optical or microwave band for microwave-optical transduction as shown in subplots (a)(b). The entanglement is generated via intraband two-mode squeezer  $\mathcal{S}(G)$  and anti-squeezer  $\mathcal{S}^\dagger(G')$ , squeezed before the traditional nonlinear coupling and antisqueezed afterwards, as shown in subplot (c). Such intraband entanglement is much easier to implement than cross-band entanglement required in teleportation-based transducers [25, 43]. For example, microwave squeezers have been well established via Josephson parametric amplifier (JPA) [52–54]. Optical entanglement has been readily generated using potassium

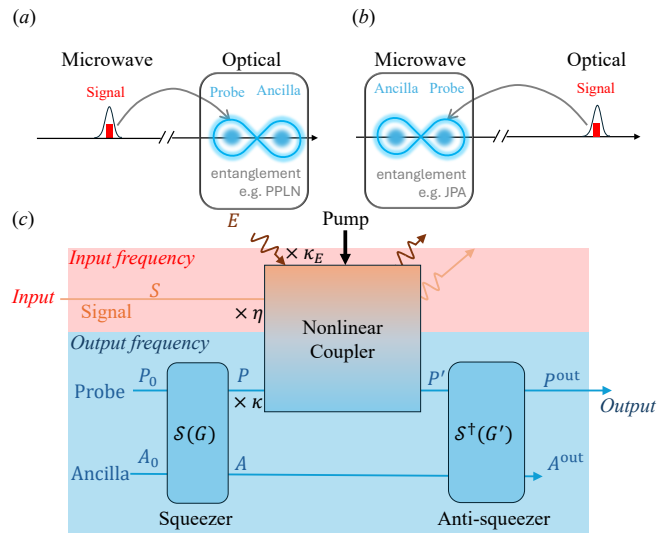


Figure 1. Schematic of the entanglement-assisted (EA) transduction protocol. (a) EA microwave-to-optical transduction, enhanced by optical entanglement which can be generated by periodically-poled lithium niobate (PPLN) [56]. (b) EA optical-to-microwave transduction, enhanced by microwave entanglement which can be generated by Josephson parametric amplifier (JPA) [52–54]. (c) Detailed protocol. An input signal  $S$  is converted to an output probe  $P^{\text{out}}$  at a different frequency. The probe and ancilla are initially cooled to vacuum state, and two-mode squeezed by  $\mathcal{S}(G)$  of gain  $G$ . Then, the signal is cast onto the probe by a nonlinear coupler, which is modelled as a beamsplitter of transmissivity  $\kappa$ , signal-probe conversion efficiency  $\eta$ , and loss  $\kappa_E = 1 - \kappa - \eta$ . Finally the probe and ancilla are antisqueezed by  $\mathcal{S}^\dagger(G')$ , the probe is output while the ancilla is discarded.

titanyl phosphate [55] and periodically-poled lithium niobate (PPLN) [56], while optical inline squeezers are also being actively developed [57, 58]. While in subplots (a)(b), we explicitly consider optical-microwave transduction, in subplot (c) we choose not to specify the input and output frequencies in our protocol, since the protocol allows general bosonic transduction, including phonon-photon conversion [59].

The pumped nonlinear coupler can be described by a linearized input-output relation, specifically a two-mode bosonic Gaussian channel which can be categorized into beamsplitter-type or two-mode-squeezing-type depending on the pump detuning, for both the cavity electro-optic coupling [16] and the cavity electro-optomechanical coupling [60]. Our analysis focuses on beamsplitter-type nonlinear couplers, of which the pumps are red-detuned, which avoid the two-mode squeezing noise [30, 36] and allow noiseless quantum transduction.

The performance of noiseless quantum transduction is characterized by the signal-to-probe photon conversion efficiency  $\eta(\omega)$ , as a function of the signal frequency  $\omega$ . The broadband performance can be quantified by the

EBP

$$\mathcal{B} \equiv \int_{-\infty}^{\infty} \eta(\omega) d\omega \quad (1)$$

or the broadband quantum capacity [61–65]

$$Q_1 = \int \frac{d\omega}{2\pi} \max \left[ \log_2 \left( \frac{\eta(\omega)}{1 - \eta(\omega)} \right), 0 \right], \quad (2)$$

of which fundamental limits can be proven for beamsplitter-type quantum transducers. In terms of EBP, we prove fundamental limits in Section IV (see Theorem 2 and Theorem 3), as summarized in Theorem 1.

**Theorem 1** (*informal summary*) *The EBP of an electro-optical transducer  $\mathcal{B}$  is upper bounded by  $\mathcal{B} \leq \pi|g\alpha|$ , limited by the nonlinear coupling coefficient  $g$  and in-cavity pump power  $|\alpha|^2$ , regardless of cavity linewidths. Enhanced by a mechanical mediating mode, the EBP of an electro-optomechanical transducer is still upper bounded similarly by nonlinear coupling coefficients and pump power.*

Such fundamental limits hold for any nonlinear couplings of similar Hamiltonians. In terms of quantum capacity, it is known that cooperativity of electro-optical transduction cavity needs to overcome a threshold  $C_{\text{th}} = 3 - 2\sqrt{2}$  to enable any non-zero capacity [43]. These fundamental limits create a conundrum in balancing pump power and heating in quantum transduction engineering.

Our main result is that these fundamental limits can be overcome by utilizing intraband entanglement. In the simple beamsplitter model of nonlinear coupling, the squeezer-coupler-antisqueezer protocol allows noiseless amplification [66, 67] of the nonlinear coupling, capable of boosting an arbitrarily low transduction efficiency to unity. In the full cavity model, in terms of the quantum capacity, the cooperativity threshold can be lowered by a factor of  $C_{\text{th,EA}} \sim 1/G$  proportional to the two-mode squeezing gain  $G$ , relaxing the requirement of cavity engineering drastically. In terms of EBP, the proposed entanglement-assisted transduction protocol enables  $\mathcal{B}_{\text{EA}} \sim G \cdot \mathcal{B}$ , allowing a factor of  $G$  advantage in EBP.

Our paper is organized as the following. We begin with the beamsplitter model of coupling in Section III to introduce the core mechanism of the protocol and analyze the advantage at a single frequency. Then, we connect the simplified model to the physical cavity model in Section IV, where we derive the fundamental limits on transduction and show these limits can be overcome by intraband entanglement.

### III. BEAMSPLITTER MODEL OF COUPLING

#### A. Protocol design

As shown in Fig. 1(c), a general bosonic transducer converts an input signal  $S$  to an output probe  $P'$  at

different frequency bands via a nonlinear coupler. A general model for quantum transduction is a frequency-dependent beamsplitter [11, 16, 34, 60]. Given a specific input frequency, the coupling can be modelled by a beamsplitter [68]. Without entanglement assistance, the transduction efficiency is limited by the signal-probe photon conversion efficiency  $\eta$ . The transmissivity of the initial probe  $P$  is  $\kappa \leq 1 - \eta$ , as a loss port  $E$  is inevitably mixed in with transmissivity (the intrinsic loss)  $\kappa_E = 1 - \kappa - \eta \geq 0$ . Its input-output relation in Fourier frequency domain is

$$\hat{\mathcal{E}}_{P'} = e^{i\theta_P} \sqrt{\kappa} \hat{\mathcal{E}}_P + e^{i\theta_S} \sqrt{\eta} \hat{\mathcal{E}}_S + \sqrt{\kappa_E} \hat{\mathcal{E}}_E, \quad (3)$$

where  $\theta_P, \theta_S$  are phase shifts during the coupling. We will connect such a beamsplitter model to the physical cavity electro-optics and electro-optomechanical systems in Sec. IV.

To enhance the overall quantum transduction efficiency from the input to the output, we amplify the signal-carrying probe while keeping the noise background in vacuum state. To suppress the noise, we introduce an ancilla  $A$ . The ancilla and the probe runs a ‘squeezer-coupler-antisqueezer’ protocol with a sandwich structure for the transducer: first the probe  $P$  and the ancilla  $A$  are cooled to vacuum states and entangled by a two-mode squeezer with gain  $G$ ; then, a portion  $\eta$  of the signal  $S$  is converted to the probe  $P'$  via nonlinear coupling; finally, the converted probe  $P'$  and the ancilla  $A$  are anti-squeezed with gain  $G'$  to produce the final converted output  $P^{\text{out}}$ . The anti-squeezer is set to null the probe back to vacuum when the input is vacuum.

Below, we elaborate this protocol step by step. Before the signal-probe coupling, we prepare the probe and the ancilla using a two-mode squeezer  $\mathcal{S}(G)$  of gain  $G$  on initial vacuums  $P_0$  and  $A_0$ . The input-output relation can be conveniently expressed via the linear transform of the field operators

$$\begin{aligned} \hat{\mathcal{E}}_P &= \sqrt{G} \hat{\mathcal{E}}_{P_0} + \sqrt{G-1} \hat{\mathcal{E}}_{A_0}^\dagger, \\ \hat{\mathcal{E}}_A &= \sqrt{G-1} \hat{\mathcal{E}}_{P_0}^\dagger + \sqrt{G} \hat{\mathcal{E}}_{A_0}. \end{aligned} \quad (4)$$

Here  $\hat{\mathcal{E}}_X(\omega)$  is the traveling-wave field operator of system  $X$  at frequency  $\omega$  relative to its own carrier, satisfying the commutation relation  $[\hat{\mathcal{E}}_X(\omega), \hat{\mathcal{E}}_X^\dagger(\omega')] = \delta(\omega - \omega')$ . In this section, we focus on the beamsplitter model at a single frequency and omit  $\omega$  for simplicity, while the broadband case will be discussed later in the full cavity model. After the two-mode squeezing, the signal is coupled to the probe via the nonlinear coupler by Eq. (3). Finally, the probe and the ancilla are anti-squeezed using  $\mathcal{S}^\dagger(G')$  to output

$$\hat{\mathcal{E}}_{P^{\text{out}}} = e^{-i\theta_P} \sqrt{G'} \hat{\mathcal{E}}_{P'} - \sqrt{G'-1} \hat{\mathcal{E}}_A^\dagger, \quad (5)$$

where the phase is chosen to cancel the transduction phase shifts  $\theta_P$  in Eq. (3). The full formula of the overall input-output relation can be found as Eq. (A3) in Appendix A. To minimize the transduction noise, we solve

$G'$  to keep the output to vacuum when the input signal is vacuum, which gives

$$G' \leftarrow G'^* \equiv \frac{1}{1 - \kappa + \kappa/G}. \quad (6)$$

In this case, the noise background in the output probe is vacuum

$$\hat{\mathcal{E}}_{P_{\text{out}}}^* = \sqrt{\eta_{\text{EA}}} e^{i(\theta_S - \theta_P)} \hat{\mathcal{E}}_S + \sqrt{1 - \eta_{\text{EA}}} \hat{\mathcal{E}}_{\text{VAC}}, \quad (7)$$

where the background  $\hat{\mathcal{E}}_{\text{VAC}}$  is in vacuum state, and

$$\eta_{\text{EA}} = \eta G'^* = \eta \frac{G}{G(1 - \kappa) + \kappa}, \quad (8)$$

is the noiseless entanglement-assisted (EA) transduction efficiency. It is noteworthy that the transduction efficiency enhancement holds even if the probe and ancilla are initially in thermal states, wherein the background  $\hat{\mathcal{E}}_{\text{VAC}}$  will be in a thermal state instead.

One can regard the two-mode anti-squeezer  $\mathcal{S}^\dagger(G')$  as an amplifier of the probe, while the first input two-mode squeezer  $\mathcal{S}(G)$  reduces the amplifier noise [67] from the anti-squeezer. Eq. (6) indicates that to increase the signal amplification  $G'$  noiselessly, the input squeezer gain  $G$  needs to increase accordingly to suppress the amplification noise. Below, our analysis begins with the ideal lossless case where  $\kappa_E = 0$  and then proceeds to the lossy case of  $\kappa_E > 0$ .

### B. Lossless coupler: unity-efficiency transduction

Now we assume the lossless limit  $\kappa_E = 0$  to gain intuition about the protocol design, which is always true at the cavity overcoupling limit (see Section IV). In this case,  $\kappa = 1 - \eta$  and the optimal gain in Eq. (6) reduces to  $G' \leftarrow G'^* \equiv 1/[\eta + (1 - \eta)/G]$ . The EA transduction efficiency is

$$\eta_{\text{EA}}|_{\kappa_E=0} = \eta \cdot \frac{G}{G\eta + (1 - \eta)}, \quad (9)$$

which approaches unity in the strong squeezing limit,

$$\eta_{\text{EA}}|_{\kappa_E=0} \rightarrow 1, \text{ when } G' \rightarrow 1/\eta \text{ and } G \rightarrow \infty. \quad (10)$$

At this limit, the output probe  $\hat{\mathcal{E}}_{P_{\text{out}}}^* = e^{i(\theta_S - \theta_P)} \hat{\mathcal{E}}_S$  is reflectionless in both quadratures. For a finite gain, the EA protocol increases the efficiency to  $\eta_{\text{EA}} \simeq G\eta$  by the amplifier gain factor  $G$ , at the weak nonlinear coupling limit  $\eta \ll 1$ . Note that here no-cloning [69] is not violated because the other output of the nonlinear coupler is infinitely noisy at the  $G \rightarrow \infty$  limit.

To enable quantum communication with one-way quantum capacity  $Q_1 > 0$ , one needs the overall conversion efficiency above the *zero-quantum-capacity threshold*,  $\eta_{\text{EA}} > 1/2$  [33], leading to  $\eta > 1/(G + 1)$  which is drastically easier to achieve than the non-EA case of  $\eta > 1/2$ .

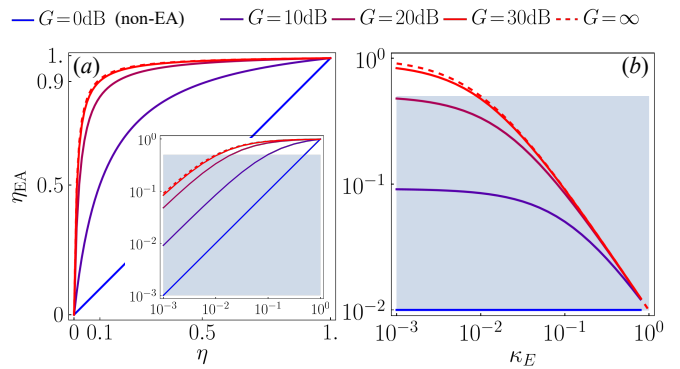


Figure 2. The EA transduction efficiency  $\eta_{\text{EA}}$  versus: (a) the non-EA efficiency  $\eta$ , with  $\kappa_E = 0.01$ ; (b) the intrinsic loss  $\kappa_E$ , with  $\eta = 0.01$ . Inset in (a): Zoom-in near  $\eta \rightarrow 0$  in logarithmic scale. Squeezer gain  $G$ : from blue to red,  $G$  increases from 0dB (non-EA) to 30dB by step of 10dB. Red dashed:  $G \rightarrow \infty$  [Eq. (11)]. Blue-shaded region: zero quantum-capacity region  $\eta_{\text{EA}} \leq 1/2$ . Anti-squeezer gain  $G'$  is chosen according to Eq. (6).

### C. Lossy coupler

Here we consider general case with intrinsic loss  $\kappa_E > 0$ . In the strong squeezing limit, the EA transduction efficiency Eq. (8) goes to

$$\eta_{\text{EA}} \rightarrow \frac{1}{1 + \kappa_E/\eta}, \text{ when } G' \rightarrow 1/(1 - \kappa) \text{ and } G \rightarrow \infty. \quad (11)$$

The challenging non-EA zero-quantum-capacity threshold  $\eta > 1/2$  is relaxed to the EA threshold  $\eta > \kappa_E$  now, which is always achievable via overcoupling the cavity.

We evaluate the EA advantage in transduction efficiency in Fig. 2. In subplot (a), we fix the intrinsic loss  $\kappa_E = 0.01$  and vary the non-EA efficiency  $\eta$ . The entanglement-assisted efficiency overwhelms the non-EA efficiency (blue diagonal line), even with an intermediate-scale, near-term available squeezing gain  $G = 10\text{dB}$ . In the inset, we observe the entanglement-assisted efficiency  $\eta_{\text{EA}}$  surpasses the zero-quantum-capacity threshold  $1/2$  (upper boundary of blue-shaded region) at  $\eta \gtrsim \kappa_E = 0.01$ , given squeezing gain  $G = 30\text{dB}$ —as predicted by Eq. (11). In subplot (b), we fix  $\eta = 0.01$  and vary  $\kappa_E$ . At high squeezing, the zero-quantum-capacity threshold  $\eta_{\text{EA}} = 1/2$  can be achieved for  $\kappa_E \lesssim \eta = 0.01$ . For the minimum squeezing requirement, we observe that at least  $G = 20\text{dB}$  is required for  $\eta_{\text{EA}} \geq 1/2$  in the best case  $\kappa_E \rightarrow 0$ , which can be predicted by the ideal cavity formula Eq. (9).

## IV. FULL CAVITY MODEL OF COUPLING

Now we proceed to the full cavity model for the nonlinear couplers. Without loss of generality, we consider on the cavity electro-optical coupling [16, 29, 32] and

electro-optomechanical coupling [11, 34]. To begin with, we focus on electro-optical transduction system, and then proceed to electro-optomechanical transduction system in Section IV C.

In cavity electro-optics, probe  $P$  and signal  $S$  are carried on optical/microwave cavity modes, associated with annihilation operators  $\hat{a}_P$ ,  $\hat{a}_S$  satisfying the commutation relation  $[\hat{a}_X, \hat{a}_X^\dagger] = 1$ , where  $X = P, S$ . The quality of the cavities are characterized by the cavity external coupling rates and intrinsic loss rates  $\gamma_{X,c}$  and  $\gamma_{X,0}$ . In this paper, we adopt the alternative characterization with the total linewidths  $\Gamma_X \equiv \gamma_{X,c} + \gamma_{X,0}$  and the coupling ratios  $\zeta_X \equiv \gamma_{X,c}/\Gamma_X$ . In the frame rotating with the cavity resonance frequencies, assuming the rotating wave approximation, an electro-optics system in the red sideband pumping case can be described by the effective Hamiltonian [16]:

$$\hat{H}_I = -\hbar g(\alpha^* \hat{a}_S^\dagger \hat{a}_P + \alpha \hat{a}_S \hat{a}_P^\dagger), \quad (12)$$

where  $g$  is the electro-optic nonlinear coupling coefficient in the unit of Hz and  $\alpha$  is the in-cavity pump amplitude. The interaction strength is typically characterized by the cooperativity  $C = 4|g\alpha|^2/\Gamma_S\Gamma_P$ .

Solving the steady-state solution of the quantum Langevin equation [16, 70] for  $\hat{H}_I$  in the Fourier domain, we obtain the broadband version of Eq. (3). The probe transmissivity spectrum is

$$\sqrt{\kappa(\omega)}e^{i\theta_P(\omega)} = -1 + \frac{2\zeta_P(1 - 2i\frac{\omega}{\Gamma_S})}{(1 - 2i\frac{\omega}{\Gamma_P})(1 - 2i\frac{\omega}{\Gamma_S}) + C}, \quad (13)$$

the signal-to-probe transduction efficiency spectrum is

$$\sqrt{\eta(\omega)}e^{i\theta_S(\omega)} = \frac{2i\sqrt{C}\sqrt{\zeta_P\zeta_S}}{(1 - 2i\frac{\omega}{\Gamma_P})(1 - 2i\frac{\omega}{\Gamma_S}) + C}. \quad (14)$$

The intrinsic loss spectrum can be obtained correspondingly as  $\kappa_E(\omega) = 1 - \kappa(\omega) - \eta(\omega)$ . It is worthwhile to note that the cavity is asymptotically lossless ( $\kappa_E(\omega) \rightarrow 0$ ) at the cavity overcoupling limit ( $\zeta_P, \zeta_S \rightarrow 1$ ). For weak nonlinear coupling  $C \ll 1$ , the peak conversion efficiency  $\eta(\omega = 0) = \zeta_P\zeta_S \cdot 4C/(1+C)^2$ ; the half-power bandwidth of  $\eta(\omega)$  is  $B \simeq \min\{\Gamma_S, \Gamma_P\}/2$ .

Now we demonstrate the quantum advantage. For simplicity, we assume a broadband two-mode squeezing for the squeezer  $G(\omega) = G$ ; for the gain in the anti-squeezing, however, the optimal choice of phase matching  $\theta_P(\omega)$  and gain  $G'^*(\omega)$  in Eq. (6) will be frequency dependent. Nevertheless, these requirements can be achieved by properly engineering the squeezing cavities. In particular, frequency-dependent squeezing is already being utilized in Laser Interferometer Gravitational-Wave Observatory (LIGO) [71]. According to Eq. (8), the EA transduction efficiency is  $\eta_{EA}(\omega) = \eta(\omega)G/[G(1 - \kappa(\omega)) + \kappa(\omega)]$ . At the  $G \rightarrow \infty$  limit, we obtain a closed-form expression

$$\eta_{EA}(\omega)|_{G \rightarrow \infty} = \frac{C\Gamma_S^2\zeta_S}{\Gamma_S^2(C + 1 - \zeta_P) + 4\omega^2(1 - \zeta_P)}. \quad (15)$$

With entanglement assistance, we observe an improvement in the peak efficiency  $\eta_{EA}(\omega = 0)|_{G \rightarrow \infty} = \zeta_S/[1 + (1 - \zeta_P)/C]$ , and a bandwidth broadening  $B_{EA}|_{G \rightarrow \infty} = \sqrt{1 + C/(1 - \zeta_P)}\Gamma_S/2$ . Remarkably, the EA bandwidth no longer depends on the probe linewidth  $\Gamma_P$  at  $G \rightarrow \infty$ . Hence the EA advantage is not limited to the weak nonlinear coupling scenarios: even though the on-resonance efficiency can get close to unity with stronger pumping merely, entanglement allows broadband improvement via bandwidth broadening. Similar quantum advantages using non-classical probes have been found in cavity dark matter searches [44, 72].

We plot an example of the EA conversion efficiency spectrum  $\eta_{EA}(\omega)$  in Fig. 3(a). As predicted, we see that the bandwidth of the non-EA case ( $G = 0$ dB) is approximately  $\Gamma_S/2$ , and the EA bandwidth grows as  $G$  increases in addition to the peak efficiency advantage.

Below, we quantify the EA advantage with three measures of transduction performance: efficiency-bandwidth product, minimum threshold of cooperativity for quantum communication, and broadband quantum capacity.

#### A. Fundamental limit on efficiency-bandwidth product

To quantify the broadband transduction efficiency, we define efficiency-bandwidth product (EBP) as the integration of transduction efficiency over the entire spectrum (see Eq. (1)). This metric is particularly useful for broadband quantum sensing applications [44].

**Theorem 2** (*EBP limit for electro-optical transduction*) *Without entanglement assistance, the EBP of quantum transduction with Hamiltonian Eq. (12) is*

$$\mathcal{B} \equiv \int_{-\infty}^{\infty} \eta(\omega)d\omega = \frac{2\pi C\Gamma_P\Gamma_S\zeta_P\zeta_S}{(C + 1)(\Gamma_P + \Gamma_S)} \leq \mathcal{B}_{\max}, \quad (16)$$

which achieves the maximum  $\mathcal{B}_{\max} \equiv \pi\zeta_S\zeta_P|g\alpha| \leq \pi|g\alpha|$ , at  $\Gamma_P = \Gamma_S = 2|g\alpha|$  (i.e.  $C = 1$ ) given a fixed  $|g\alpha|$ .

$\mathcal{B}_{\max}$  is a fundamentally limit for the non-EA case determined by the nonlinear coupling coefficient  $g$  and pump power  $\propto |\alpha|^2$ , which is independent on any higher- $Q$  cavity engineering. For electro-optomechanical transducers, we present a similar limit in Section IV C.

Meanwhile, we also derive a closed-form expression of EA EBP  $\mathcal{B}_{EA} \equiv \int_{-\infty}^{\infty} \eta_{EA}(\omega)d\omega$ , which is too lengthy to be displayed here. Under the same cavity setup  $\Gamma_P = \Gamma_S = 2|g\alpha|$ ,  $\zeta_P = \zeta_S = 1$ , we obtain  $\mathcal{B}_{EA} = G^{1/4}\pi|g\alpha| \geq G^{1/4}\mathcal{B}_{\max}$ , breaking the fundamental limit  $\mathcal{B}_{\max}$  of the non-EA case. Allowing freely choosing  $\Gamma_P = \Gamma_S = 2\sqrt{G}|g\alpha|$ , we have  $\mathcal{B}_{EA} \simeq 0.703\sqrt{G}\pi|g\alpha|$  with  $\sqrt{G}$  advantage compared to  $\mathcal{B}_{\max}$ . When  $G \rightarrow \infty$ ,

$$\mathcal{B}_{EA}|_{G \rightarrow \infty} \rightarrow \frac{\pi C\Gamma_S\zeta_S}{2\sqrt{(1 + C - \zeta_P)(1 - \zeta_P)}}, \quad (17)$$

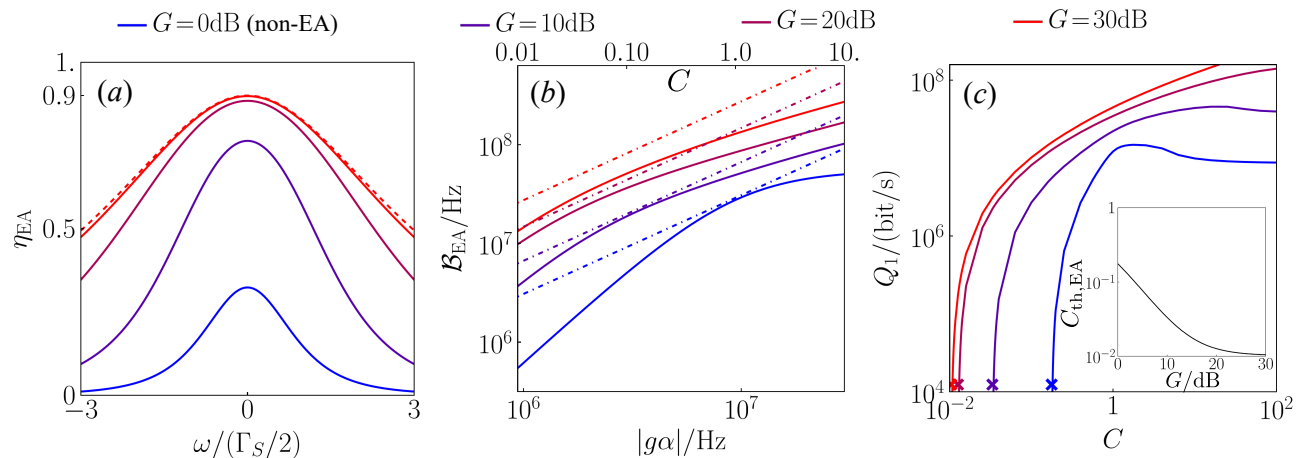


Figure 3. (a) EA transduction efficiency spectrum  $\eta_{\text{EA}}(\omega)$  under various squeezing gain  $G$ . Cooperativity  $C = 0.1$ . The dashed line is the  $G \rightarrow \infty$  limit obtained from Eq. (15). (b) The EA efficiency-bandwidth product  $\mathcal{B}_{\text{EA}}$  versus the effective nonlinear coupling strength  $|g\alpha|$ . The solid lines are under fixed  $\Gamma_P, \Gamma_S$ , for which we provide the cooperativity  $C$  values as the upper axis ticks; while the dot-dashed lines are under optimized  $\Gamma_P, \Gamma_S$  that maximize  $\mathcal{B}_{\text{EA}}$  for a given  $|g\alpha|$ . (c) Broadband quantum capacity rate  $Q_1$  versus cooperativity  $C$  under various squeezing gain  $G$ . The crosses indicate the zero-quantum-capacity thresholds  $C_{\text{th}}$  under each  $G$  in Eq. (19). Inset:  $C_{\text{th}}$  versus  $G$ (dB), as given in Eq. (19). The  $G = 0$ dB point goes back to Eq. (18). In all figures,  $\zeta_P = \zeta_S = 0.99$ ; Linewidths  $\Gamma_P = 25.8$ MHz,  $\Gamma_S = 13.706$ MHz are chosen according to the high-cooperativity setup in Ref. [29], except the dot-dash lines of (b).

which diverges as  $\zeta_P \rightarrow 1$  as expected.

While the above optimal results provide the ultimate limits, here we also consider the practical case of low cooperativity  $C \ll 1$ . In this case, entanglement can enhance EBP by a factor of  $G$ ,  $\mathcal{B}_{\text{EA}} = G \cdot \mathcal{B}$  when  $\zeta_P = \zeta_S = 1$ .

Under imperfect  $\zeta_P, \zeta_S < 1$ , we plot  $\mathcal{B}_{\text{EA}}$  in Fig. 3(b). Still, we observe orders of magnitude of EA advantage. Either with  $\Gamma_S, \Gamma_P$  fixed (solid lines) or with optimized  $\Gamma_S, \Gamma_P$  over each given  $|g\alpha|$  (dot-dashed lines), the EA advantages are demonstrated over the maximal non-EA EBP  $\mathcal{B}_{\text{max}}$  (blue dot-dashed line) over a wide range of effective nonlinear coupling strength  $|g\alpha|$ , corresponding to cooperativity  $C \in [0.01, 10]$  for the  $\Gamma_S, \Gamma_P$  fixed cases.

### B. Threshold of cooperativity and broadband quantum information rate

While the efficiency-bandwidth product provides an intuitive characterization of the transduction efficiency, the ultimate quantum information transmission rates are characterized by the quantum capacity [61–63] across the entire spectrum. When the environment are cooled to vacuum, the one-way quantum capacity of transducer is given by Eq. (2) [64, 65].

At the weak nonlinear coupling limit, the maximum transduction efficiency locates at the on-resonance frequency  $\omega = 0$ . For the non-EA case, we have  $\eta(0) = 4C\zeta_P\zeta_S/(1+C)^2$  which surpasses the zero-

capacity threshold  $1/2$  only when [43]

$$C \geq C_{\text{th}} = -1 + 4\zeta_S\zeta_P - \sqrt{8\zeta_S\zeta_P(2\zeta_S\zeta_P - 1)} \geq 3 - 2\sqrt{2}. \quad (18)$$

With the EA boost, we have the threshold

$$C_{\text{th,EA}} = -1 + \zeta_P((4\zeta_S - 2)G + 2) - 2\sqrt{\zeta_P G(\zeta_P(4\zeta_S + (1 - 2\zeta_S)^2 G - 1) - 2\zeta_S)}. \quad (19)$$

When  $G \rightarrow \infty$ , the threshold converges to  $C_{\text{th}} \rightarrow (1 - \zeta_P)/(2\zeta_S - 1)$  when  $\zeta_S \geq 1/2$ .

Additional insight can be obtained by considering the overcoupling limit of  $\zeta_P = \zeta_S = 1$ , threshold in Eq. (19) leads to  $C_{\text{th,EA}}|_{\zeta_P=\zeta_S=1} = 1/(\sqrt{G} + \sqrt{1+G})^2$ , which is lowered by a factor of  $1/G$  asymptotically. It is easy to check that  $\eta_{\text{EA}}(0)$  approaches unity at the large  $G$  limit. We plot the threshold in the inset of Fig. 3(c) for a practical case and identify a reduction by over an order of magnitude when squeezing gain  $G$  is large.

We plot  $Q_1$  versus the cooperativity  $C$  for different gain  $G$  in Fig. 3(c). Merely  $G = 10$ dB squeezing is sufficient to enable orders of magnitude advantage at low cooperativity. Remarkably, for large  $C$  the quantum capacity without probe-ancilla entanglement begins to decay with  $C$  as the cavity goes into the oscillatory region with Rabi splitting; in contrast, the quantum capacity assisted by probe-ancilla entanglement can further increase with  $C \gg 1$ .

### C. Generalization to transduction with intermediate modes

Microwave-optical quantum transduction is known to be enhanced by mediating modes. As an example, we focus on the electro-optomechanical transduction, which yields the state-of-the-art efficiency so far [30]. In the frame rotating at the cavity resonance frequencies for microwave and optical modes, the cavity electro-optomechanical dynamics can be described by the effective Hamiltonian [11, 70, 73]

$$H_I = \hbar g_S \hat{a}_S^\dagger \hat{a}_S \hat{x}_M + \hbar g_P \hat{a}_P^\dagger \hat{a}_P \hat{x}_M \quad (20)$$

where  $\hat{a}_S, \hat{a}_P, \hat{a}_M$  are the annihilation operators of the signal (microwave/optical), probe (optical/microwave), and mediating (mechanical) modes, and  $\hat{x}_M = x_{zp}(\hat{a}_M + \hat{a}_M^\dagger)$  with  $x_{zp} = \sqrt{\frac{\hbar}{2m\omega_M}}$  being the zero-point motion. The mechanical oscillator has mass  $m$  and frequency  $\omega_M$ . Here the nonlinear coupling coefficients  $g_S, g_P$  are in unit of  $\text{Hz} \cdot \text{m}^{-1}$ . We define  $\mathcal{G}_{S,P} \equiv g_{S,P} x_{zp} |\alpha_{S,P}|$  proportional to the nonlinear coupling coefficients and pumping amplitudes, analogous to  $g|\alpha|$  in the electro-optical coupling [16].

Consider red sideband pumping and the resolved sideband limit, the electro-optomechanical coupling yields the beamsplitter-type input-output relation similar to the electro-optics, up to a different spectral lineshape. Thus most of our conclusions for the electro-optics can be trivially generalized to the electro-optomechanics. Here we present the EBP limit.

**Theorem 3** (*EBP limit for electro-optomechanical transduction*) *Without entanglement assistance, the EBP of quantum transduction with Hamiltonian Eq. (20) is upper bounded by Eq. (C10) as a function of  $\mathcal{G}_P, \mathcal{G}_S$ .*

*Specifically, in the symmetric case of  $\mathcal{G}_P = \mathcal{G}_S = \mathcal{G}$ , the EBP is upper bounded by*

$$\mathcal{B}_{\mathcal{G}_P=\mathcal{G}_S} \leq \frac{\sqrt{107+51\sqrt{17}}}{32} \pi \zeta_P \zeta_S \mathcal{G} \simeq 1.749 \zeta_P \zeta_S \mathcal{G}. \quad (21)$$

Our EA transduction protocol also applies to electro-optomechanical transduction. Similar enhancement in EBP proportional to two-mode squeezing gain  $G$  can overcome the above fundamental EBP limit. At the over-coupling limit  $\zeta_P, \zeta_S \rightarrow 1$  and lossless mechanical resonator, the overall coupling loss  $\kappa_E(\omega) \rightarrow 0$ , then the signal can always be perfectly recovered with strong squeezing  $G \rightarrow \infty$  as  $\eta_{\text{EA}}(\omega)|_{\kappa_E \rightarrow 0, G \rightarrow \infty} \rightarrow 1$ .

## V. DISCUSSIONS

The most challenging part of the proposed EA transduction is a frequency-dependent inline squeezing. In the optical-to-microwave transduction, the required microwave inline squeezing can be readily realized to

high gain [52–54]. Alternative to realizing optical inline squeezing for microwave-to-optical transduction, one can also utilize the optical-to-microwave transduction to generate optical-microwave entanglement from optical-optical entanglement [74, 75], then teleportation enables bi-directional transduction [25, 43].

In this paper we have focused on the beamsplitter-type nonlinear couplers. We expect the intraband entanglement to similarly enhance the squeezing-type couplers, which we leave to future study. We note that the squeezing-type transducers cannot perform any quantum transduction without our proposal of intraband entanglement assistance, because it forms a phase-conjugate amplifier of zero quantum capacity [60, 76].

Finally, we address the superiority of our proposal to the existing works. Compared with the proposal with in-cavity squeezing [77] that boosts a single quadrature transduction, our approach allows transduction of both quadratures thus is free from encoding in the ideal case, and does not require additional pumping at the cavity that can lead to additional heating. Moreover, an explicit protocol that recovers the initial quantum state is absent in Ref. [77]. Compared with the GKP-based protocol in Ref. [40] that requires the input signal to be GKP encoded, our protocol relies on less challenging quantum resources of inline squeezing. Distinct from both the two protocols above, our proposal lifts the requirement of encoding and thus can be applied to transduce general bosonic quantum states more compatible with existing optical communication infrastructures. While Ref. [40] only considers the perfect cavity of  $\kappa_E = 0$ , our protocol shows advantage for general scenarios. Compared with the adaptive protocol [39], our protocol does not require the precise broadband homodyne measurement and adaptive control, which typically requires delay lines that increase the loss and limit the capacity and speed of transduction. We note that our proposal requires two-mode squeezers, as well as the single-mode squeezers in Ref. [39], of which the bandwidth are being actively increased [54, 56, 78].

## ACKNOWLEDGMENTS

The project is supported by Office of Naval Research Grant No. N00014-23-1-2296 and National Science Foundation Engineering Research Center for Quantum Networks Grant No. 1941583. QZ also acknowledges support from DARPA MeasQUIT HR0011-24-9-036, National Science Foundation OMA-2326746 and National Science Foundation CAREER Award CCF-2240641. HS and QZ proposed the protocol in discussion, performed analyses, generated the figures and wrote the manuscript.

### Appendix A: Full derivation of the overall input-output relation of entanglement-assisted transducer

Consider initial probe and ancilla modes  $\hat{\mathcal{E}}_{P_0}, \hat{\mathcal{E}}_{A_0}$  in vacuum. The two-mode squeezer before nonlinear coupling gives

$$\begin{aligned}\hat{\mathcal{E}}_P &= \sqrt{G}\hat{\mathcal{E}}_{P_0} + \sqrt{G-1}\hat{\mathcal{E}}_{A_0}^\dagger, \\ \hat{\mathcal{E}}_A &= \sqrt{G-1}\hat{\mathcal{E}}_{P_0}^\dagger + \sqrt{G}\hat{\mathcal{E}}_{A_0}.\end{aligned}\quad (\text{A1})$$

The nonlinear coupling forms a beamsplitter between the squeezed probe  $\hat{\mathcal{E}}_P$  and the signal  $\hat{\mathcal{E}}_S$ :

$$\hat{\mathcal{E}}_{P'} = e^{i\theta_P} \sqrt{\kappa} \hat{\mathcal{E}}_P + e^{i\theta_S} \sqrt{\eta} \hat{\mathcal{E}}_S + \sqrt{\kappa_E} \hat{\mathcal{E}}_E, \quad (\text{A2})$$

while ancilla  $\hat{\mathcal{E}}_A$  is intact. Here, the intrinsic loss  $\kappa_E = 1 - \eta - \kappa$  and the environment mode  $\hat{\mathcal{E}}_E$  is in vacuum. After the nonlinear coupling, the antisqueezer, with phase compensation  $-\theta_P$  on probe, gives the final output

$$\begin{aligned}\hat{\mathcal{E}}_{P_{\text{out}}} &= e^{-i\theta_P} \sqrt{G'} \hat{\mathcal{E}}_{P'} - \sqrt{G'-1} \hat{\mathcal{E}}_A^\dagger \\ &= e^{-i\theta_P} \sqrt{G'} \left( e^{i\theta_P} \sqrt{\kappa} \hat{\mathcal{E}}_P + e^{i\theta_S} \sqrt{\eta} \hat{\mathcal{E}}_S + \sqrt{\kappa_E} \hat{\mathcal{E}}_E \right) \\ &\quad - \sqrt{G'-1} \hat{\mathcal{E}}_A^\dagger \\ &= \left( \sqrt{G\kappa G'} - \sqrt{(G'-1)(G-1)} \right) \hat{\mathcal{E}}_{P_0} \\ &\quad + e^{i(\theta_S - \theta_P)} \sqrt{\eta G'} \hat{\mathcal{E}}_S \\ &\quad + \left( \sqrt{(G-1)\kappa G'} - \sqrt{(G'-1)G} \right) \hat{\mathcal{E}}_{A_0}^\dagger \\ &\quad + e^{-i\theta_P} \sqrt{(1-\eta-\kappa)} G' \hat{\mathcal{E}}_E.\end{aligned}\quad (\text{A3})$$

To keep the output to vacuum when the input signal is vacuum, one needs to annihilate the coefficient in front of  $\hat{\mathcal{E}}_{A_0}^\dagger$  in Eq. (A3), leading to

$$G' \leftarrow G'^* \equiv \frac{1}{1 - \kappa + \kappa/G}. \quad (\text{A4})$$

By such antisqueezing, finally the output reduces to

$$\hat{\mathcal{E}}_{P_{\text{out}}}^* = \frac{\sqrt{\kappa} \hat{\mathcal{E}}_{P_0} + \sqrt{\eta G} e^{i(\theta_S - \theta_P)} \hat{\mathcal{E}}_S + \sqrt{(1-\eta-\kappa)G} e^{-i\theta_P} \hat{\mathcal{E}}_E}{\sqrt{G(1-\kappa) + \kappa}}. \quad (\text{A5})$$

Note that  $\hat{\mathcal{E}}_{P_0}, \hat{\mathcal{E}}_E$  are in vacuum state, the output can be written as

$$\hat{\mathcal{E}}_{P_{\text{out}}}^* = \sqrt{\eta_{\text{EA}}} e^{i(\theta_S - \theta_P)} \hat{\mathcal{E}}_S + \sqrt{1 - \eta_{\text{EA}}} \hat{\mathcal{E}}_{\text{VAC}}, \quad (\text{A6})$$

where the noise background  $\hat{\mathcal{E}}_{\text{VAC}}$  is in vacuum state, we define the entanglement-assisted (EA) transduction efficiency as

$$\eta_{\text{EA}} \equiv \frac{\eta G}{G(1-\kappa) + \kappa}. \quad (\text{A7})$$

### Appendix B: Full derivation of EBP of electro-optical transduction

To solve the EBP, we make use of the integration formula

$$\int_{-\infty}^{\infty} d\omega \frac{1}{C_1 + 4\omega^2 C_2 + 16\omega^4} = \frac{\pi}{\sqrt{2}\sqrt{C_1}\sqrt{C_2 + 2\sqrt{C_1}}}. \quad (\text{B1})$$

Without the EA [see Eq. (14)], we have

$$\eta(\omega) = \frac{4C\Gamma_P^2 \Gamma_S^2 \zeta_P \zeta_S}{(C+1)^2 \Gamma_P^2 \Gamma_S^2 + 4\omega^2 (-2C\Gamma_P \Gamma_S + \Gamma_P^2 + \Gamma_S^2) + 16\omega^4}. \quad (\text{B2})$$

With EA and optimal  $G'$  [see Eq. (8)], we have

$$\eta_{\text{EA}}(\omega) =$$

$$\frac{4C\Gamma_P^2 \Gamma_S^2 \zeta_P \zeta_S G}{\Gamma_P^2 \Gamma_S^2 (4(C+1)\zeta_P(G-1) + (C+1)^2 - 4\zeta_P^2(G-1)) + 4\omega^2 (-2C\Gamma_P \Gamma_S + \Gamma_S^2 + \Gamma_P^2 (4\zeta_P(\zeta_P - \zeta_P G + G - 1) + 1)) + 16\omega^4}. \quad (\text{B3})$$

At the overcoupling limit of  $\zeta_P = \zeta_S = 1$ , the above formula simplifies to

$$\eta_{\text{EA}}(0)|_{\zeta_P=\zeta_S=1} = \eta(0) \frac{G}{[1 + 4(G-1)C/(C+1)^2]}. \quad (\text{B4})$$



Now consider cooperativity  $C = 4|g\alpha|^2/\Gamma_S\Gamma_P$ , we fix the pump power and the nonlinear coupling coefficient, and consider EBP as a function of the cavity parameters  $\Gamma_S, \Gamma_P$ . With Eq. (B1), we have without EA

$$\mathcal{B} \equiv \int_{-\infty}^{\infty} \eta(\omega) d\omega = \frac{2\pi C \Gamma_P \Gamma_S \zeta_P \zeta_S}{C \Gamma_P + C \Gamma_S + \Gamma_P + \Gamma_S} = 8\pi |g\alpha| \zeta_P \zeta_S \frac{\tilde{\Gamma}_P \tilde{\Gamma}_S}{(\tilde{\Gamma}_P + \tilde{\Gamma}_S)(4 + \tilde{\Gamma}_P \tilde{\Gamma}_S)}, \quad (\text{B5})$$

where we have defined  $\tilde{\Gamma}_X = \Gamma_X/|g\alpha|$ .

For the EA formula, we can also obtain lengthy closed-form solution of EA EBP  $\mathcal{B}_{\text{EA}} \equiv \int_{-\infty}^{\infty} \eta_{\text{EA}}(\omega) d\omega$  from Eq. (B1), which we will not display here. For  $\zeta_P = \zeta_S = 1$ , we have a slightly simpler result,

$$\mathcal{B}_{\text{EA}} = \frac{8\pi \tilde{\Gamma}_P \tilde{\Gamma}_S G |g\alpha|}{\sqrt{(\tilde{\Gamma}_P \tilde{\Gamma}_S (\tilde{\Gamma}_P \tilde{\Gamma}_S + 16G - 8) + 16) \left( \tilde{\Gamma}_P^2 + \tilde{\Gamma}_S^2 + 2\sqrt{\tilde{\Gamma}_P \tilde{\Gamma}_S (\tilde{\Gamma}_P \tilde{\Gamma}_S + 16G - 8) + 16} - 8 \right)}}. \quad (\text{B6})$$

### Appendix C: Electro-optomechanical transduction

The cavity electro-optomechanical dynamics can be described by the full Hamiltonian [11, 70, 73]

$$H = \hbar\omega_S \hat{a}_S^\dagger \hat{a}_S + \hbar\omega_P \hat{a}_P^\dagger \hat{a}_P + \hbar\omega_M \hat{a}_M^\dagger \hat{a}_M + \hbar g_S \hat{a}_S^\dagger \hat{a}_S \hat{x}_M + \hbar g_P \hat{a}_P^\dagger \hat{a}_P \hat{x}_M \quad (\text{C1})$$

where  $\hat{a}_S, \hat{a}_P, \hat{a}_M$  are the annihilation operators of the signal (microwave), probe (optical), and mediating (mechanical) modes,  $\hat{x}_M = x_{\text{zp}}(\hat{a}_M + \hat{a}_M^\dagger)$  with  $x_{\text{zp}} = \sqrt{\frac{\hbar}{2m\omega_M}}$ , the frequencies of signal, probe and mediating modes are denoted as  $\omega_S, \omega_P$  and  $\omega_M$ . Here the nonlinear coupling coefficients  $g_S, g_P$  (of electro-mechanical and optomechanical couplings respectively) are in unit of  $\text{Hz} \cdot \text{m}^{-1}$ . (In the brackets we take the microwave-to-optical transduction as an example). We define  $\mathcal{G}_{S,P} \equiv g_{S,P} x_{\text{zp}} |\alpha_{S,P}|$  proportional to the nonlinear coupling coefficients and the pumping amplitudes, analogous to  $g|\alpha|$  in the electro-optical coupling [16].

The input-output relation is described by the Langevin equation [11, 70, 73]. Below we summarize the solution of Langevin equation for cavity electro-optomechanical transduction.

#### 1. Input-output relation

Consider input field operator vector  $\hat{\mathcal{E}}_{in} \equiv [\hat{\mathcal{E}}_{S,in}, \hat{\mathcal{E}}_{S,E}, \hat{\mathcal{E}}_{P,in}, \hat{\mathcal{E}}_{P,E}, \hat{\mathcal{E}}_{M,E}, \hat{\mathcal{E}}_{S,in}^\dagger, \hat{\mathcal{E}}_{S,E}^\dagger, \hat{\mathcal{E}}_{P,in}^\dagger, \hat{\mathcal{E}}_{P,E}^\dagger, \hat{\mathcal{E}}_{M,E}^\dagger]^T$ , where  $\hat{\mathcal{E}}_{S,in}, \hat{\mathcal{E}}_{P,in}$  are input fields at signal and probe frequencies respectively,  $\hat{\mathcal{E}}_{S,E}, \hat{\mathcal{E}}_{P,E}, \hat{\mathcal{E}}_{M,E}$  are environment fields at signal, probe, and mediating frequencies respectively. And similarly output field operator vector  $\hat{\mathcal{E}}_{out} \equiv [\hat{\mathcal{E}}_{S,out}, \hat{\mathcal{E}}_{P,out}, \hat{\mathcal{E}}_{S,out}^\dagger, \hat{\mathcal{E}}_{P,out}^\dagger]^T$ . Also the cavity mode annihilation operator vector  $\hat{\mathbf{a}} \equiv [\hat{a}_S, \hat{a}_P, \hat{a}_M, \hat{a}_S^\dagger, \hat{a}_P^\dagger, \hat{a}_M^\dagger]^T$ . With strong pumps, the Langevin equation is linearized as

$$\frac{d}{dt} \hat{\mathbf{a}}(t) = A \hat{\mathbf{a}}(t) + B \hat{\mathcal{E}}_{in}(t), \quad \hat{\mathcal{E}}_{out}(t) = C \hat{\mathbf{a}}(t) + D \hat{\mathcal{E}}_{in}(t), \quad (\text{C2})$$

where

$$\begin{aligned}
A &= \begin{pmatrix} -\frac{\Gamma_S}{2} + i\Delta_S & 0 & i\mathcal{G}_S & 0 & 0 & i\mathcal{G}_S \\ 0 & -\frac{\Gamma_P}{2} + i\Delta_P & i\mathcal{G}_P & 0 & 0 & i\mathcal{G}_P \\ i\mathcal{G}_S & i\mathcal{G}_P & -\frac{\Gamma_M}{2} - i\omega_M & i\mathcal{G}_S & i\mathcal{G}_P & 0 \\ 0 & 0 & -i\mathcal{G}_S & -\frac{\Gamma_S}{2} - i\Delta_S & 0 & -i\mathcal{G}_S \\ 0 & 0 & -i\mathcal{G}_P & 0 & -\frac{\Gamma_P}{2} - i\Delta_P & -i\mathcal{G}_P \\ -i\mathcal{G}_S & -i\mathcal{G}_P & 0 & -i\mathcal{G}_S & -i\mathcal{G}_P & -\frac{\Gamma_M}{2} + i\omega_M \end{pmatrix}, \\
B &= \begin{pmatrix} \sqrt{\gamma_{S,c}} & \sqrt{\gamma_{S,0}} & 0 & 0 & 0 & 0 & 0 & 0 & 0 & 0 \\ 0 & 0 & \sqrt{\gamma_{P,c}} & \sqrt{\gamma_{P,0}} & 0 & 0 & 0 & 0 & 0 & 0 \\ 0 & 0 & 0 & 0 & \sqrt{\Gamma_M} & 0 & 0 & 0 & 0 & 0 \\ 0 & 0 & 0 & 0 & 0 & \sqrt{\gamma_{S,c}} & \sqrt{\gamma_{S,0}} & 0 & 0 & 0 \\ 0 & 0 & 0 & 0 & 0 & 0 & 0 & \sqrt{\gamma_{P,c}} & \sqrt{\gamma_{P,0}} & 0 \\ 0 & 0 & 0 & 0 & 0 & 0 & 0 & 0 & 0 & \sqrt{\Gamma_M} \end{pmatrix}, \\
C &= \begin{pmatrix} \sqrt{\gamma_{S,c}} & 0 & 0 & 0 & 0 & 0 \\ 0 & \sqrt{\gamma_{P,c}} & 0 & 0 & 0 & 0 \\ 0 & 0 & 0 & \sqrt{\gamma_{S,c}} & 0 & 0 \\ 0 & 0 & 0 & 0 & \sqrt{\gamma_{P,c}} & 0 \end{pmatrix}, \quad D = \begin{pmatrix} -1 & 0 & 0 & 0 & 0 & 0 & 0 & 0 & 0 & 0 \\ 0 & 0 & -1 & 0 & 0 & 0 & 0 & 0 & 0 & 0 \\ 0 & 0 & 0 & 0 & 0 & -1 & 0 & 0 & 0 & 0 \\ 0 & 0 & 0 & 0 & 0 & 0 & 0 & -1 & 0 & 0 \end{pmatrix}.
\end{aligned} \tag{C3}$$

where  $\gamma_{S,0}, \gamma_{S,c}$  are the intrinsic loss rate and the coupling rate of the signal cavity, similar for  $\gamma_{P,0}, \gamma_{P,c}$  of the probe cavity, total linewidth  $\Gamma_S = \gamma_{S,0} + \gamma_{S,c}, \Gamma_P = \gamma_{P,0} + \gamma_{P,c}, \Delta_S, \Delta_P$  are the detunings of the pumps from the resonance frequencies for signal and probe cavities respectively. We define the coupling ratios  $\zeta_P \equiv \gamma_{P,c}/\Gamma_P, \zeta_S \equiv \gamma_{S,c}/\Gamma_S$ . In the steady-state limit, it is convenient to consider the frequency spectrum of the input-output relation. Fourier transform of the Langevin equation gives

$$\hat{\mathcal{E}}_{out}(\omega) = S(\omega)\hat{\mathcal{E}}_{in}(\omega) \tag{C4}$$

where  $\omega$  is the frequency at the frame rotating with the pump frequencies of signal and probe, the spectral transfer matrix  $S(\omega) = C(-i\omega I_6 - A)^{-1}B + D$ ,  $I_6$  is a  $6 \times 6$  identity matrix.

Now consider the red sideband detuning  $\Delta_S = \Delta_P = -\omega_M$  to maximize the noiseless beamsplitter-type conversion and suppress the noisy blue sideband squeezing-type conversion [30, 60]. From Eq. (C4), we obtain the intrinsic conversion efficiency of electro-optomechanical transduction at the frequency resolved limit  $\Gamma_S, \Gamma_P \ll \omega_M$ :

$$\begin{aligned}
\eta_{\text{EMO}}(\omega) &\equiv |S_{13}(\omega)|^2 \Big|_{\Delta_S = \Delta_P = -\omega_M; \Gamma_S, \Gamma_P \ll \omega_M} \\
&= \frac{64\mathcal{G}_P^2 \mathcal{G}_S^2 \Gamma_P \zeta_P \Gamma_S \zeta_S}{4\Delta\omega^2 (4\mathcal{G}_P^2 + 4\mathcal{G}_S^2 + \Gamma_M \Gamma_P + \Gamma_M \Gamma_S + \Gamma_P \Gamma_S - 4\Delta\omega^2)^2 + (4\mathcal{G}_S^2 \Gamma_P + 4\mathcal{G}_P^2 \Gamma_S - 4\Delta\omega^2 (\Gamma_M + \Gamma_P + \Gamma_S) + \Gamma_M \Gamma_P \Gamma_S)^2}
\end{aligned} \tag{C5}$$

where  $\Delta\omega \equiv \omega - \omega_M$ .

## 2. EBP

The transduction efficiency Eq. (C5) has six pure imaginary poles in three pairs  $p_1, p_2, p_3, p_4 = -p_1, p_5 = -p_2, p_6 = -p_3$ , of which the formulas are too lengthy to be shown here. Thus, the spectral integral gives the EBP

$$\mathcal{B}^{\text{EMO}} \equiv \int_{-\infty}^{\infty} \eta_{\text{EMO}}(\omega) d\omega = \frac{i\pi (p_1 + p_2 + p_3) \mathcal{G}_P^2 \mathcal{G}_S^2 \Gamma_P \Gamma_S \zeta_P \zeta_S}{(p_1 + p_2)(p_1 + p_3)(p_2 + p_3)p_1 p_2 p_3}. \tag{C6}$$

Here  $\mathcal{B}^{\text{EMO}}$  is always real as the imaginary sign in the numerator cancels with the imaginary signs of the poles. We find that  $\mathcal{B}^{\text{EMO}}$  is maximized at  $\Gamma_M \rightarrow 0$ , given finite cooperativity  $C_S = 4\mathcal{G}_S^2/\Gamma_S \Gamma_m, C_P = 4\mathcal{G}_P^2/\Gamma_P \Gamma_m$ . In this case,  $p_1 \simeq i\frac{\Gamma_M(C_P+C_S+1)}{2}, p_2 \simeq \frac{i\Gamma_P}{2}, p_3 \simeq \frac{i\Gamma_S}{2}$ , which gives

$$\mathcal{B}^{\text{EMO}}|_{\Gamma_M \rightarrow 0} \simeq \frac{8\pi\mathcal{G}_P^2 \mathcal{G}_S^2 \Gamma_P^2 \zeta_P \Gamma_S^2 \zeta_S (4\mathcal{G}_P^2 \Gamma_S + 4\mathcal{G}_S^2 \Gamma_P + \Gamma_P \Gamma_S (\Gamma_P + \Gamma_S))}{(\Gamma_P + \Gamma_S) (\mathcal{G}_P^2 \Gamma_S + \mathcal{G}_S^2 \Gamma_P) (4\mathcal{G}_P^2 \Gamma_S + \Gamma_P (4\mathcal{G}_S^2 + \Gamma_P \Gamma_S)) (4\mathcal{G}_P^2 \Gamma_S + \Gamma_P (4\mathcal{G}_S^2 + \Gamma_S^2))}. \tag{C7}$$

In the symmetric case of  $\mathcal{G}_P = \mathcal{G}_S = \mathcal{G}$ , we can obtain the maximum analytically

$$\mathcal{B}_{\text{max}}^{\text{EMO}} = \frac{\sqrt{107 + 51\sqrt{17}}}{32} \pi \zeta_P \zeta_S \mathcal{G} \simeq 1.749 \zeta_P \zeta_S \mathcal{G}. \tag{C8}$$

In the general case of  $\mathcal{G}_P \neq \mathcal{G}_S$ , exact maximization is in general challenging. By eliminating terms in the denominator, we find the EBP is upper bounded by

$$\mathcal{B}^{\text{EMO}}|_{\Gamma_M \rightarrow 0} \leq \pi \zeta_P \zeta_S [4\mathcal{G}_P^2 \Gamma_S + 4\mathcal{G}_S^2 \Gamma_P + \Gamma_P \Gamma_S (\Gamma_P + \Gamma_S)] \cdot \min \left\{ \frac{\mathcal{G}_S^2 \Gamma_P^2}{2\mathcal{G}_P^4 \Gamma_S^2}, \frac{\mathcal{G}_P^2 \Gamma_S^2}{2\mathcal{G}_S^4 \Gamma_P^2}, \frac{8\mathcal{G}_S^2}{\Gamma_S^3 \Gamma_P} \right\} \equiv \mathcal{B}_{\text{UB}}^{\text{EMO}}, \quad (\text{C9})$$

which is maximized to a finite value over any cavity linewidth  $\Gamma_S, \Gamma_P$

$$\mathcal{B}_{\text{UB,max}}^{\text{EMO}} = \frac{4\pi \sqrt[8]{\mathcal{G}_P \mathcal{G}_S} \zeta_P \zeta_S \left( (\mathcal{G}_P \mathcal{G}_S)^{3/4} + \sqrt[4]{\mathcal{G}_P \mathcal{G}_S^5} + \mathcal{G}_P^{3/2} + \mathcal{G}_S^{3/2} \right)}{\mathcal{G}_S^{5/8}} \quad (\text{C10})$$

at  $\Gamma_S \rightarrow \frac{2\mathcal{G}_S^{9/8}}{\sqrt[8]{\mathcal{G}_P}}, \Gamma_P \rightarrow \frac{2\mathcal{G}_P^{11/8}}{\mathcal{G}_S^{3/8}}$ , where the coupling ratios  $\zeta_P, \zeta_S \leq 1$ . As a reminder, here  $\mathcal{G}_P, \mathcal{G}_S$  are analogous to  $|g\alpha|$  of electro-optical coupling which are independent on cavity quality factor or coupling rate. Hence, similar to the electro-optical transducers, the EBP of electro-optomechanical transducers is fundamentally limited regardless of any cavity engineering.

We note that our result of  $\mathcal{B}_{\text{UB,max}}^{\text{EMO}}$  is not symmetric about  $S, P$  since we arbitrarily chose the terms in the denominator of  $\mathcal{B}^{\text{EMO}}|_{\Gamma_M \rightarrow 0}$  to eliminate, which leads to a loose upper bound  $\mathcal{B}_{\text{UB}}^{\text{EMO}}$ . More careful choices are likely to offer a tighter upper bound.

- 
- [1] N. Lauk, N. Sinclair, S. Barzanjeh, J. P. Covey, M. Saffman, M. Spiropulu, and C. Simon, *Quantum Sci. Techno.* **5**, 020501 (2020).
- [2] D. Awschalom, K. K. Berggren, H. Bernien, S. Bhawe, L. D. Carr, P. Davids, S. E. Economou, D. Englund, A. Faraon, M. Fejer, *et al.*, *PRX Quantum* **2**, 017002 (2021).
- [3] X. Han, W. Fu, C.-L. Zou, L. Jiang, and H. X. Tang, *Optica* **8**, 1050 (2021).
- [4] A. Acín, J. I. Cirac, and M. Lewenstein, *Nat. Phys.* **3**, 256 (2007).
- [5] H. J. Kimble, *Nature* **453**, 1023 (2008).
- [6] S. Wehner, D. Elkouss, and R. Hanson, *Science* **362** (2018).
- [7] W. Kozłowski and S. Wehner, in *Proceedings of the Sixth Annual ACM International Conference on Nanoscale Computing and Communication* (2019) pp. 1–7.
- [8] Z. Zhang and Q. Zhuang, *Quantum Sci. Techno.* **6**, 043001 (2021).
- [9] C. Monroe, R. Raussendorf, A. Ruthven, K. R. Brown, P. Maunz, L.-M. Duan, and J. Kim, *Phys. Rev. A* **89**, 022317 (2014).
- [10] S. Barz, E. Kashefi, A. Broadbent, J. F. Fitzsimons, A. Zeilinger, and P. Walther, *Science* **335**, 303 (2012).
- [11] R. W. Andrews, R. W. Peterson, T. P. Purdy, K. Cicak, R. W. Simmonds, C. A. Regal, and K. W. Lehnert, *Nat. Phys.* **10**, 321 (2014).
- [12] J. Bochmann, A. Vainsencher, D. D. Awschalom, and A. N. Cleland, *Nat. Phys.* **9**, 712 (2013).
- [13] A. Vainsencher, K. Satzinger, G. Peairs, and A. Cleland, *Appl. Phys. Lett.* **109**, 033107 (2016).
- [14] K. C. Balram, M. I. Davanço, J. D. Song, and K. Srinivasan, *Nat. Photonics* **10**, 346 (2016).
- [15] M. Tsang, *Phys. Rev. A* **81**, 063837 (2010).
- [16] M. Tsang, *Phys. Rev. A* **84**, 043845 (2011).
- [17] L. Fan, C.-L. Zou, R. Cheng, X. Guo, X. Han, Z. Gong, S. Wang, and H. X. Tang, *Sci. Adv.* **4**, eaar4994 (2018).
- [18] Y. Xu, A. A. Sayem, L. Fan, S. Wang, R. Cheng, C.-L. Zou, W. Fu, L. Yang, M. Xu, and H. X. Tang, *arXiv:2012.14909* (2020).
- [19] W. Jiang, C. J. Sarabalis, Y. D. Dahmani, R. N. Patel, F. M. Mayor, T. P. McKenna, R. Van Laer, and A. H. Safavi-Naeini, *Nat. Commun.* **11**, 1 (2020).
- [20] J. Verdú, H. Zoubi, C. Koller, J. Majer, H. Ritsch, and J. Schmiedmayer, *Phys. Rev. Lett.* **103**, 043603 (2009).
- [21] L. A. Williamson, Y.-H. Chen, and J. J. Longdell, *Phys. Rev. Lett.* **113**, 203601 (2014).
- [22] L. Shao, M. Yu, S. Maity, N. Sinclair, L. Zheng, C. Chia, A. Shams-Ansari, C. Wang, M. Zhang, K. Lai, *et al.*, *Optica* **6**, 1498 (2019).
- [23] N. Fiaschi, B. Hensen, A. Wallucks, R. Benevides, J. Li, T. P. M. Alegre, and S. Gröblacher, *Nat. Photon.* **15**, 817 (2021).
- [24] X. Han, W. Fu, C. Zhong, C.-L. Zou, Y. Xu, A. Al Sayem, M. Xu, S. Wang, R. Cheng, L. Jiang, *et al.*, *Nat. Commun.* **11**, 1 (2020).
- [25] C. Zhong, Z. Wang, C. Zou, M. Zhang, X. Han, W. Fu, M. Xu, S. Shankar, M. H. Devoret, H. X. Tang, *et al.*, *Phys. Rev. Lett.* **124**, 010511 (2020).
- [26] M. Mirhosseini, A. Sipahigil, M. Kalaei, and O. Painter, *Nature* **588**, 599 (2020).
- [27] M. Forsch, R. Stockill, A. Wallucks, I. Marinković, C. Gärtner, R. A. Norte, F. van Otten, A. Fiore, K. Srinivasan, and S. Gröblacher, *Nat. Phys.* **16**, 69 (2020).
- [28] J. Holzgrafe, N. Sinclair, D. Zhu, A. Shams-Ansari, M. Colangelo, Y. Hu, M. Zhang, K. K. Berggren, and M. Lončar, *Optica* **7**, 1714 (2020).
- [29] R. Sahu, W. Hease, A. Rueda, G. Arnold, L. Qiu, and J. M. Fink, *Nat. Commun.* **13**, 1276 (2022).
- [30] B. M. Brubaker, J. M. Kindem, M. D. Urmey, S. Mittal, R. D. Delaney, P. S. Burns, M. R. Vissers, K. W. Lehnert, and C. A. Regal, *Phys. Rev. X* **12**, 021062 (2022).

- [31] L. Qiu, R. Sahu, W. Hease, G. Arnold, and J. M. Fink, *Nat. Commun.* **14**, 3784 (2023).
- [32] R. Sahu, L. Qiu, W. Hease, G. Arnold, Y. Minoguchi, P. Rabl, and J. M. Fink, *Science* **380**, 718 (2023).
- [33] M. M. Wolf, D. Pérez-García, and G. Giedke, *Phys. Rev. Lett.* **98**, 130501 (2007).
- [34] A. P. Higginbotham, P. Burns, M. Urmeý, R. Peterson, N. Kampel, B. Brubaker, G. Smith, K. Lehnert, and C. Regal, *Nat. Phys.* **14**, 1038 (2018).
- [35] W. Hease, A. Rueda, R. Sahu, M. Wulf, G. Arnold, H. G. Schwefel, and J. M. Fink, *PRX Quantum* **1**, 020315 (2020).
- [36] C. M. Caves, *Phys. Rev. D* **26**, 1817 (1982).
- [37] S. M. Meenehan, J. D. Cohen, S. Gröblacher, J. T. Hill, A. H. Safavi-Naeini, M. Aspelmeyer, and O. Painter, *Phys. Rev. A* **90**, 011803 (2014).
- [38] H. Zhao, W. D. Chen, A. Kejriwal, and M. Mirhosseini, *arXiv preprint arXiv:2406.02704* (2024).
- [39] M. Zhang, C.-L. Zou, and L. Jiang, *Phys. Rev. Lett.* **120**, 020502 (2018).
- [40] Z. Wang and L. Jiang, *arXiv:2401.16781* (2024).
- [41] S. Konno, W. Asavanant, F. Hanamura, H. Nagayoshi, K. Fukui, A. Sakaguchi, R. Ide, F. China, M. Yabuno, S. Miki, *et al.*, *Science* **383**, 289 (2024).
- [42] S. Meesala, S. Wood, D. Lake, P. Chiappina, C. Zhong, A. D. Beyer, M. D. Shaw, L. Jiang, and O. Painter, *Nat. Phys.* , 1 (2024).
- [43] J. Wu, C. Cui, L. Fan, and Q. Zhuang, *Phys. Rev. Appl.* **16**, 064044 (2021).
- [44] H. Shi and Q. Zhuang, *npj Quantum Inf.* **9**, 27 (2023).
- [45] F. Hudelist, J. Kong, C. Liu, J. Jing, Z. Ou, and W. Zhang, *Nat. Commun.* **5**, 3049 (2014).
- [46] M. Chekhova and Z. Ou, *Adv. Opt. Photonics* **8**, 104 (2016).
- [47] S. Guha and B. I. Erkmen, *Phys. Rev. A* **80**, 052310 (2009).
- [48] K. Wurtz, B. Brubaker, Y. Jiang, E. Ruddy, D. Palken, and K. Lehnert, *PRX Quantum* **2**, 040350 (2021).
- [49] S. Hao, H. Shi, C. N. Gagatsos, M. Mishra, B. Bash, I. Djordjevic, S. Guha, Q. Zhuang, and Z. Zhang, *Phys. Rev. Lett.* **129**, 010501 (2022).
- [50] Y. Jiang, E. P. Ruddy, K. O. Quinlan, M. Malnou, N. E. Frattini, and K. W. Lehnert, *PRX Quantum* **4**, 020302 (2023).
- [51] K. A. Gilmore, M. Affolter, R. J. Lewis-Swan, D. Barberena, E. Jordan, A. M. Rey, and J. J. Bollinger, *Science* **373**, 673 (2021).
- [52] K. M. Backes, D. A. Palken, S. A. Kenany, B. M. Brubaker, S. Cahn, A. Droster, G. C. Hilton, S. Ghosh, H. Jackson, S. K. Lamoreaux, *et al.*, *Nature* **590**, 238 (2021).
- [53] M. Xu, R. Cheng, Y. Wu, G. Liu, and H. X. Tang, *PRX Quantum* **4**, 010322 (2023).
- [54] J. Y. Qiu, A. Grimsmo, K. Peng, B. Kannan, B. Lienhard, Y. Sung, P. Krantz, V. Bolkhovskiy, G. Calusine, D. Kim, *et al.*, *Nat. Phys.* **19**, 706 (2023).
- [55] T. Eberle, V. Händchen, and R. Schnabel, *Optics express* **21**, 11546 (2013).
- [56] R. Nehra, R. Sekine, L. Ledezma, Q. Guo, R. M. Gray, A. Roy, and A. Marandi, *Science* **377**, 1333 (2022).
- [57] Z. Yan, X. Jia, X. Su, Z. Duan, C. Xie, and K. Peng, *Phys. Rev. A* **85**, 040305 (2012).
- [58] M. Wang, M. Zhang, Z. Qin, Q. Zhang, L. Zeng, X. Su, C. Xie, and K. Peng, *Laser & Photonics Rev.* **16**, 2200336 (2022).
- [59] A. H. Safavi-Naeini and O. Painter, *New J. Phys.* **13**, 013017 (2011).
- [60] C. L. Rau, A. Kyle, A. Kwiatkowski, E. Shojaei, J. D. Teufel, K. W. Lehnert, and T. Dennis, *Phys. Rev. Appl.* **17**, 044057 (2022).
- [61] S. Lloyd, *Phys. Rev. A* **55**, 1613 (1997).
- [62] P. W. Shor, in *lecture notes, MSRI Workshop on Quantum Computation* (2002).
- [63] I. Devetak, *IEEE Trans. Inf. Theory* **51**, 44 (2005).
- [64] A. S. Holevo and R. F. Werner, *Phys. Rev. A* **63**, 032312 (2001).
- [65] C.-H. Wang, F. Li, and L. Jiang, *Nat. Commun.* **13**, 6698 (2022).
- [66] Z. Ou, *Physical Review A* **48**, R1761 (1993).
- [67] J. Kong, F. Hudelist, Z. Ou, and W. Zhang, *Phys. Rev. Lett.* **111**, 033608 (2013).
- [68] C. Weedbrook, S. Pirandola, R. García-Patrón, N. J. Cerf, T. C. Ralph, J. H. Shapiro, and S. Lloyd, *Rev. Mod. Phys.* **84**, 621 (2012).
- [69] W. K. Wootters and W. H. Zurek, *Nature* **299**, 802 (1982).
- [70] C. W. Gardiner and M. J. Collett, *Phys. Rev. A* **31**, 3761 (1985).
- [71] L. McCuller, C. Whittle, D. Ganapathy, K. Komori, M. Tse, A. Fernandez-Galiana, L. Barsotti, P. Fritschel, M. MacInnis, F. Matichard, *et al.*, *Phys. Rev. Lett.* **124**, 171102 (2020).
- [72] M. Malnou, D. Palken, B. Brubaker, L. R. Vale, G. C. Hilton, and K. Lehnert, *Phys. Rev. X* **9**, 021023 (2019).
- [73] W. P. Bowen and G. J. Milburn, *Quantum optomechanics* (CRC press, 2015).
- [74] H. Vahlbruch, M. Mehmet, K. Danzmann, and R. Schnabel, *Phys. Rev. Lett.* **117**, 110801 (2016).
- [75] T. Kashiwazaki, N. Takanashi, T. Yamashima, T. Kazama, K. Enbutsu, R. Kasahara, T. Umeki, and A. Furusawa, *APL Photonics* **5** (2020).
- [76] A. S. Holevo, *Probl. Inf. Transm.* **44**, 171 (2008).
- [77] C. Zhong, M. Xu, A. Clerk, H. X. Tang, and L. Jiang, *Phys. Rev. Research* **4**, L042013 (2022).
- [78] Z. Yang, M. Jahanbozorgi, D. Jeong, S. Sun, O. Pfister, H. Lee, and X. Yi, *Nat. Commun.* **12**, 4781 (2021).